Available online at www.sciencedirect.com

SciVerse ScienceDirect

Physics Procedia 37 (2012) 1016 – 1023

Physics Procedia

TIPP 2011 – Technology and Instrumentation for Particle Physics 2011

Characterisation of Glasgow/CNM double-sided 3D sensors.

Aaron Mac Raighne[a*], K. Akiba[h], J. P. Balbuena[d], R. Bates[b], M. van Beuzekom[h], J. Buytaert[e], P. Collins[e], M. Crossley[e], R. Dumps[e], L. Eklund[b], C. Fleta[d], A. Gallas[f], M. Gersabeck[b], V.V. Gligorov[b], M. John[g], M. Köhler[c], M. Lozano[d], D. Maneuski[b], U. Parzefall[c], D. Quirion[d], R. Plackett[e], C. Parkes[b], G. Pellegrini[d], E. Rodrigues[b], G. Stewart[b].

a School of Physics, Dublin Institute of Technology, Kevin Street, Dublin 8, Ireland
b SUPA, School of Physics and Astronomy, University of Glasgow, Scotland, U.K.
c Physikalisches Institut, Universitt Freiburg, Germany
d Instituto de Microelectrónica de Barcelona, IMB-CNM-CSIC, Barcelona, Spain
e CERN CH-1211, Genéve 23, Switzerland
f Facultad de Fisica, University of Santiago de Compostela, Santiago de Compostela, Spain
g Dept. of Physics, University of Oxford, Oxford, U.K.
h Nationaal Instituut Voor Subatomaire Fysica, Amsterdam, Netherlands

Abstract

3D detectors are proposed as an alternative to planar silicon technology to withstand the high radiation environments in planned future high energy physics experiments. Here we review the characterization of double-sided 3D detectors designed and built at CNM and the University of Glasgow. A non-irradiated sensor is characterized in a pion test-beamutilizing the Timepix telescope. The charge collection and detection efficiency across the unit pixel are shown. Area of inefficiency can be found at the columnar electrodes at perpendicular angles of beam incidence while the pixels are shown to be fully efficient at angles greater than ten degrees. A reduction in charge sharing compared to the planar technology is also demonstrated. Charge collection studies on irradiated devices with a Sr-90 source show higher charge collection efficiency for 3D over planar sensors at significantly lower applied bias. The sub-pixel response is probed by a micro-focused laser beam demonstrating areas of charge multiplication at high bias voltages.

Keywords: 3D sensors; high energy physics detectors; radiation-hardness; silicon detectors.

 doi:10.1016/j.phpro.2012.02.445

1. Introduction

Planned luminosity upgrades to the LHC over the next ten years will create radiation environments in which current detector technology cannot withstand. In conjunction to this the experiments of the LHC will also undergo a series of upgrades [1-3]. The expected maximum fluences inside the experiments will ultimately increase ten-fold to levels close to 10^{16}cm^{-2} 1 MeV equivalent neutrons (1 MeV n_{eq} /cm^{-2}) consisting essentially of charged particles. Such doses are unprecedented for silicon detectors. New detector technologies are being investigated to deal with such high radiation fluence. One such technology is the double-sided 3D detector.

1.1. Double-sided 3D devices

The double-sided 3D detector shown in figure 1(a) [4] is a variation of the single-sided original design proposed by Parker *et al* [5]. The difference with the double-sided design is that the columnar electrodes do not traverse the full thickness of the sensor. This simplifies the fabrication process and increases the yield by removing the need to dope both electrode types from a single side of the wafer. The double-sided device also has the advantage over the single-sided 3D sensors that all regions of the sensor have active silicon, as charge is still collected in the region above or below the columnar electrodes. These regions also contain a lower field region which requires the detector to be over depleted to be fully active [6].

The devices investigated in this report were designed by the University of Glasgow and IMB-CNM and fabricated by IMB-CNM. In this design inductively coupled plasma (ICP) is used to etch 10 µm diameter holes to a depth of 250 µm in a (285±15) µm thick substrate sensor material, see figure 1(a). The high aspect ratio is made possible by an alternating sequence of etch and passivation cycles. P^+ and n^+ electrodes are produced by partially filling the holes with polysilicon and doping with boron and phosphorous respectively. A 3D detector may be constructed as either a pixel or a strip detector. The exposed electrodes can be treated for bump-bonding to a pixel chip or connected together via a metallization layer on the top of the device to be connected to strip read-out electronics. The ohmic column type are all connected together to form the bias electrode via a metallized doped polysilicon layer deposited above an oxide layer over the back side of the silicon detector. The silicon oxide layer on the back side reduces the magnitude of the electric field at the tip of the junction column and gives improved high voltage characteristics [6].

2. Pion test-beamscans of non-irradiated devices.

2.1. Experimental set-up

A planar and the 3D sensor were tested in custom built telescope in a 120 GeV pion beam provided by the Super Proton Synchrotron (SPS) at CERN. The double-sided 3D sensor consisting of an n-type substrate and p-doped columns, as shown in figure 1(a), was solder bump-bonded by VTT to a Timepix pixel readout chips. The sensors used were fabricated from a wafer of resistivity 13 kΩcm and had a leakage current of 3.8 µA at 20 V at room temperature. The planar sensors used were from a standard series of sensors produced by CANBERRA for the Medipix2 collaboration. The substrates are n-type, and the devices have p^+ electrodes for hole collection. The substrate resistivity was 32 kΩcm, corresponding to a 10 V full depletion voltage for the 300 µm thick device. The devices were solder bump-bonded by VTT to Timepix and Medipix2 readout chips.

The telescope consisted of six detector planes. The telescope detector planes consisted of four Timepix [7] and two Medipix2 [8] chips, each bonded to a standard planar 300 µm p^+-on-n and controlled by

Pixelman [9] and USB readout electronics [10] developed by the IEAP. Energy deposition in each pixel in the Timepix telescope planes is provided by the Time over Threshold (ToT) mode. This allows for a weight-centered hit position to be determined for each telescope plane and for energy deposition information in the DUTs (Device Under Test). The telescope planes were angled at 9° in both the horizontal and vertical axes perpendicular to the beam line. This angle produces multi-hit cluster and provided a pointing resolution of 2.3 µm from the telescope. The DUT was mounted on translational and rotational stages at the centre of the telescope arms. Further information on the telescope performance and the track reconstruction can be found in [11].

2.2. Charge collection and Efficiency

Energy deposition in the pixel cell is provided by the ToT mode in the Timepix chip. Figure 1(c) and (f) show the energy deposition of a particle as a function of the track position mapped onto a unit cell. Figure 1(c) shows the mean energy deposited in a unit pixel while figure 1(f) shows mean energy deposited in the cluster, combining the hit pixel with the energy deposited in its neighbours. The frequency of the collected number of ToT counts for areas of interest are shown in figures 3 (b), (d), (e) and (g).

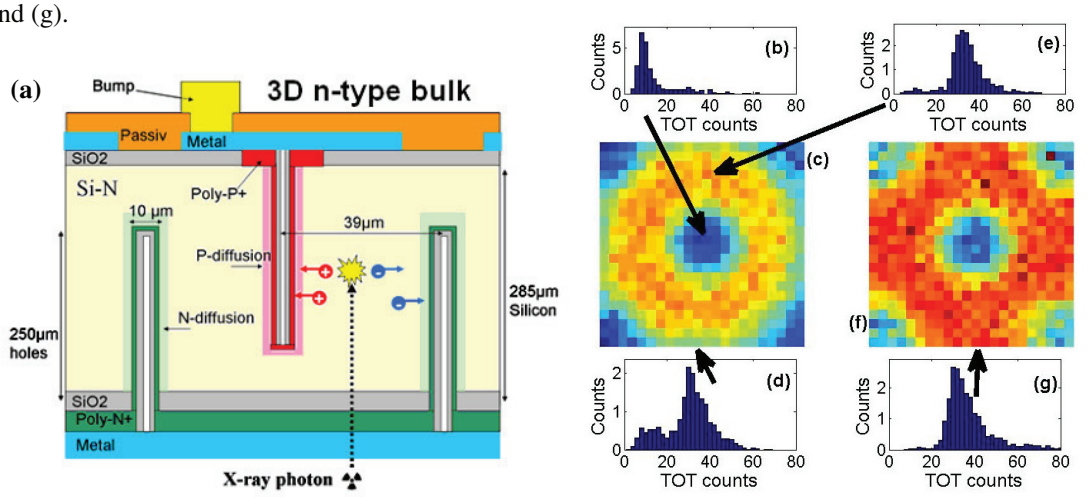

Fig. 1. (a) Schematic of the double-sided 3D sensor. Histograms of the ToT counts in the central electrode region (b), away from the central electrode and pixel edges (e). Pixel maps showing the mean energy deposition across the pixel matrix, for a single pixel (c) and the energy in clusters (f). (d) and (g) show the histograms of the energy deposited at the pixel edges for the single pixel and the clusters.

It is clear from figure 1(e) and (g) that the Landau shape expected from Minimum Ionizing Particles (MIP) can be resolved in regions of the pixel removed from the columnar electrodes. A reduced amount of charge is collected from the regions of the electrodes, see figure 1(b). Charge deposited at the edge of the pixels can be collected from neighbouring pixels to reconstruct the Landau shape expected, figure 1(d) and (g).

Figure 2(a) and (b) shows the efficiency measured across the pixel for 2 V and 20 V bias. A bias voltage of 2 V depletes the region between the columns, while 20 V fully depletes the sensor. To probe the efficiencies of the different pixel areas we define three regions. The central electrode region is defined as a 5 µm radius circular region centered on the central electrode. The corner electrodes region consists of

quarter circle areas of the same radius in the pixel corners. A 5 µm radius has been chosen here as this corresponds to the size of the etched electrode. A third region defined is the area of high counts, away from the electrode regions. This is defined as the area outside a 15 µm radius region from the corner and centre electrodes. A 15 µm radius has been chosen as this excludes all potential for reduced counts due to the electrode column size, 5 µm radius, the diffusion of the dopant into the substrate of 3 µm around the polysilicon layer [4], the smearing of the low count region by the resolution of the telescope, 2.3 µm [11], and the sensor being not quite perpendicular to the beam. Efficiencies of (99.1±0.5) and (99.7±0.5) % are measured in the regions clear from the electrodes, at 2 V and 20 V respectively. A lower efficiency of (79.1±0.5) % is measured in the region of the central electrode at 2 V but this rises to 86.7% at 20 V applied bias. Further analysis is available in [12].

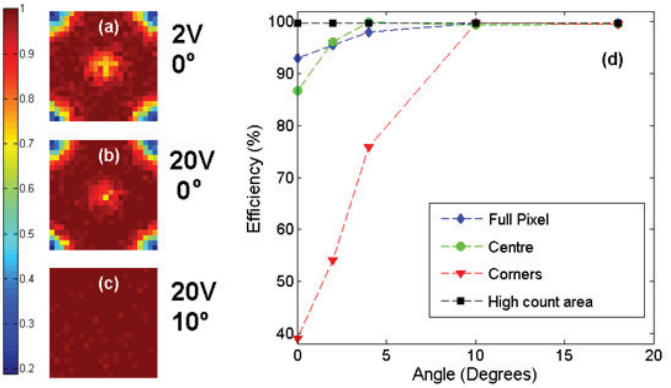

Fig. 2. Pixel maps of the efficiencies at 2V and 0° (a), 20V at 0° (b) and 20V at 10° (c) showing the fully efficient response at 10° across the entire pixel. Also shown are the efficiencies in regions of the pixel (see text) as a function of rotation angle for the sensor at 20V (d).

The efficiency map study was repeated with the DUT rotated by up to 18° around the vertical axis. In figure 1(d) the efficiencies of selected regions of the detector are shown. As the angle is increased a track traverses less of the electrode column and a greater section of the depleted silicon. At angles of 10° and higher the electrodes have no effect on the efficiency measurements and an efficiency of (99.8±0.5) % is reached across the entire pixel matrix. At an angle of 10° the track traverses a full pixel within the thickness of the sensors.

2.3. Charge sharing

Due to the electrode design in the 3D sensor the charge cloud created by a MIP will be drifted away from the pixel boundaries towards the junction electrodes. This contrasts with the planar sensor in which the charge cloud is drifted parallel to the pixel boundary. This allows the charge cloud in the planar sensor to diffuse across pixels and results in increased charge sharing. Charge sharing is useful in finding track position by weight-centered techniques however with heavily irradiated devices it is useful to collect the signal in as few pixels as possible giving higher signal to noise ratio. Figure 3 shows the positions of the track intercepts of the particles mapped onto a unit pixel cell in the detectors. Single pixel hits, hits creating clusters of two pixels and clusters containing three or more pixels are plotted separately. Both sensors were operated above full depletion, with the 3D sensor biased to 20 V and the planar sensor at 100 V. Single pixel hits in the 3D device can be found to be spread across almost the entire pixel, figure 8(a), with a slight reduction at the pixel edge and corners. In comparison the single hits in the planar device are confined to the central section of the pixel. Particles incident outside the central pixel area

share their created charge with two (f) or more (g) pixels. This is best illustrated by the ratio of multiple hit clusters to single pixel hits for the 3D (d) and planar (h) devices. 59% of incident particles share sufficient charge with neighboring pixels to create multiple pixel hits in the planar detector. This is compared with 14% in the 3D device. These charge sharing values are specific to this geometry and bias voltages: decreasing the pixel size and the bias voltages will increase the charge sharing in both devices. Evidence of a reduction in charge sharing in irradiated 3D sensors can be found in [13].

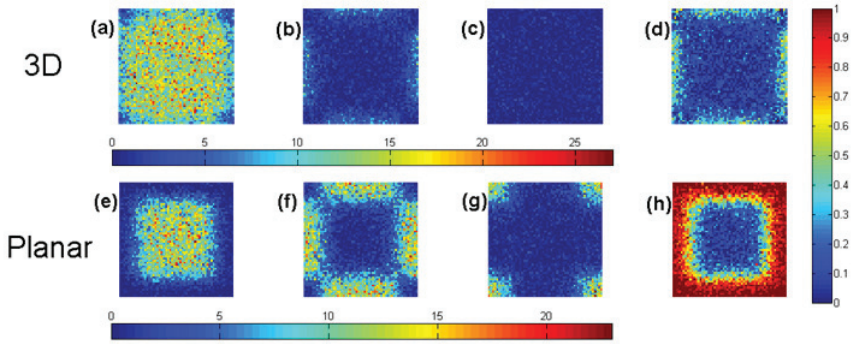

Fig. 3. Track intercept positions across the 3D pixel matrix in a single pixel cell for tracks of normal incidence, for one pixel clusters (a), for two pixels clusters (b), for clusters sizes >2 (c). The ratio of (hits>1)/(total hits) (d). Track positions across the planar pixel matrix, for one pixel clusters (e), for two pixels clusters (f), for clusters sizes >2 (g). The ratio of (hits>1)/(total hits) (h). Values in (a)-(c) and (e)-(g) are in numbers of counts.

3. Charge collection studies on irradiated 3D devices

3.1. Devices under test

3D devices produced as described in section 1.1 have their n^+ readout electrodes connected via a metallization layer resulting in strips of 80 µm pitch. To perform strip isolation a p-stop ring surrounds each n^+ junction column. The 3D strip sensors were irradiated at the Karlsruhe Institute of Technology (Germany) at -20 °C, without bias, with a flux of 26 MeV protons. The devices were irradiated to fluences of 0.5, 1, 2, 5, 10 and 20 x 10^{15} $1MeVn_{eq}cm^{-2}$. The devices were stored at -20 °C or less after the irradiation period and no intentional annealing was performed. The devices were at room temperature for typically a total of 5 days before tests were performed. P-stop isolation is measured before and after irradiation, with inter-strip resistance of ~100 MΩ. Lateral depletion voltages increases from 4 V to 100 V and 145 V for un-irradiated sensors and those irradiated to 5 and 10 x 10^{15} $1MeVn_{eq}cm^{-2}$ respectively.

Performance was compared to a set of 320 µm thick planar p-type silicon ATLAS upgrade [14] detectors irradiated by a neutron flux [15]. The sensors were measured up to the maximum possible bias voltage that could be applied before breakdown occurred (between 900 and 1000 V). The values obtained are in agreement with those published in the literature [16], performing a valuable cross-check.

3.2. Sr-90 charge collection studies

The response of the DUTs to a Sr-90 source were measured for a range of bias voltages with the analogue LHC speed Beetle readout chip [17]; integrated into the Alibava data acquisition system [18]. The temperature of the ceramics on which the DUTs were mounted kept at (-13.4±2.2) °C. For a full description of the set-up including gain calibrations please see [19].

Figure 4(a) shows the charge collection efficiency for a 3D device held at a modest bias voltage of 150 V, except for the non-irradiated sample which had a bias voltage of 50 V. This is compared with a planar device biased at the significantly higher voltage of 1000 V. The planar sensor is thicker than the 3D sensor and therefore collects a greater number of electrons when both sensors are un-irradiated. However the 3D shows greater charge collection when irradiated. Large charge collection efficiencies of 90% and 47% can be seen at $2x10^{15}$ and $10x10^{15}$ 1 MeV n_{eq} /cm^{-2} respectively. These large collection efficiencies are present for the 3D at modest voltages of 150 V compared with the planar sensor which is biased at a much higher voltage of 1,000 V. Also shown in figure 4(a) is the signal to noise ratio extracted from the 3D strip sensors. As the noise remains reasonably constant, at this bias voltage, the Signal to Noise Ratio (SNR) is seen to follow the collected charge. This gives a SNR of >10 at fluences of $10x10^{15}$ 1 MeV n_{eq} /cm^{-2}. This has been simulated using TCAD without any high field effects present and shows very good agreement [19].

Increasing the applied bias to the 3D sensor has the effect of increasing the collected charge. Figure 4(b) shows the charge collection at a higher applied bias. The bias at each position is the highest that could be reasonably applied to the sensor (between 250 and 300 V). Here the charge collected is significantly higher than at lower bias. At applied biases of 250-300 V 137% of the expected charge deposition by a Sr-90 electron is collected for a sensor irradiated to $1x10^{15}$ 1 MeV n_{eq} /cm^{-2}. Collecting more charge than is deposited clearly points towards charge multiplication inside the sensor. This may occur through band-to-band tunneling and impact ionisation. Both effects are possible in a highly biased device with high space charge density. For impact ionisation to occur in silicon the electric fields in the device must be in excess of 10^5 Vcm^{-1}. Such high voltages in the 3D sensor would be found in regions of high field such as close to and between the electrodes.

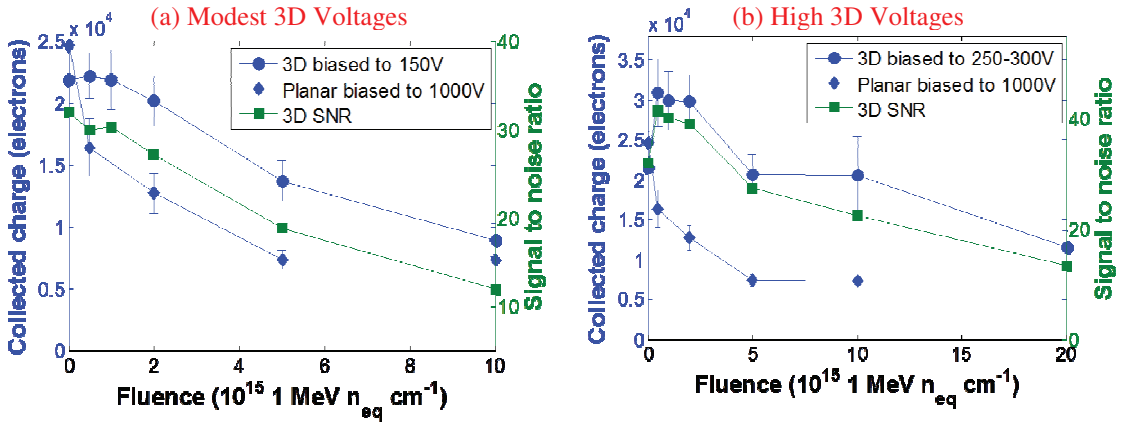

Fig.4 (a). Collected charge in electrons for a 3D sensor biased at 150 V and a planar sensor biased at 1,000 V irradiated to varying fluencies. In addition the signal to noise ratio is shown for the 3D device. (b) Similar plot to that in (b) but at higher applied bias.

3.3. Focused infra-red laser light charge collection studies

The Sr-90 measurements described above probe the average response of the detector, allowing the absolute charge collection efficiency and signal to noise ratios to be extracted. To probe the relative charge collection efficiency as a function of position in a unit cell of the device a focused laser system is employed. A 4 µm diameter focused infrared laser spot is raster scanned in 2 µm steps across the front surface of the sensor [20, 21]. As the absorption depth of the 974 nm wavelength light in silicon is about 100 µm the charge collection process in the upper portion of the detector is investigated preferentially.

Scans preformed on un-irradiated sensors match closely with those preformed on un-irradiated sensors scanned by a micro-focused x-ray beam [12, 22].

Laser scans on un-irradiated sensors show a uniform collection of charge outside of the electrode regions [19]. In contrast to this large areas of non-uniformity can be seen in the unit pixel of irradiated sensors. Figure 5(b) show the charge collected when the laser is scanned across a part of the strip as illustrated in figure 5(a). The sensor was irradiated to $2x10^{15}$ 1 MeV n_{eq}/cm^{-2} and biased at 260 V. Two areas as outlined on the schematic are the high area field, between the junction and ohmic electrodes, and the low field region, close to the mid-point between two ohmic electrodes. A higher field region will result in faster charge collection and less time for charge trapping resulting in greater charge collection. The relative signal from these regions was investigated for increasing bias voltage, shown in figure 5(c). Below 150 V an increasing voltage leads to less charge trapping and increases the charge collected in both regions. However, the increase in charge collection is modest. When the voltage is increased from 150 V to 260 V the charge collection increases dramatically. This is due to charge multiplication effects as mentioned above in Section 3.2. The difference in the signal between the high and low field regions is about 30%.

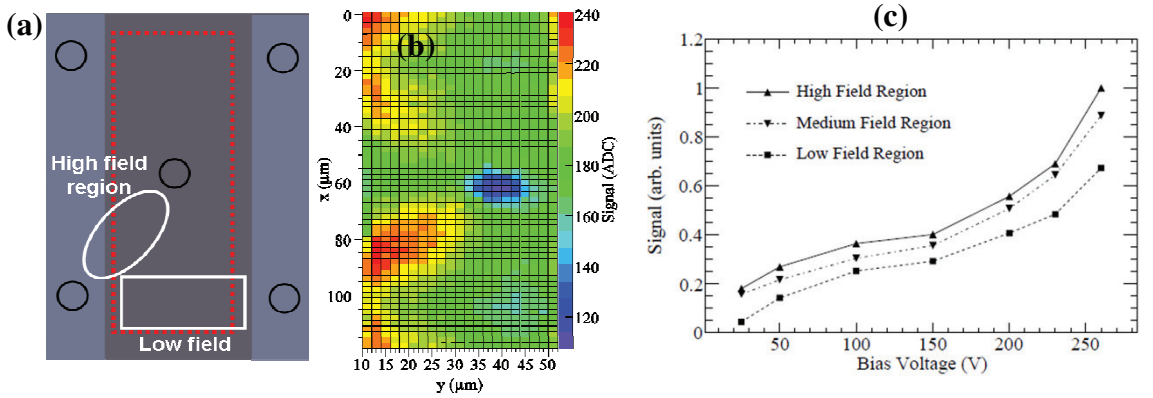

Fig. 5. (a) Schematic of a section of the 3D strip sensor, outlined in red is the scanned area of the pixel. The response of this scan is shown in (b) while the signal in the different regions marked in (a) are shown in (c).

4. Conclusions

3D sensors have been characterised with varying methods. Efficiency measurements are made with the use of a high-energy beam with the Timepix telescope. Non-irradiated devices show high detection efficiency at perpendicular angles of incidence, (93±0.5) %, and full efficiency, (99.8±0.5) %, when the detector is tilted to angles greater than 10^{o} with respect to the beam. The decrease in charge sharing of these sensors over planar technology is clearly seen through cluster analysis.

Sr-90 tests show the increased charge collection efficiency of the 3D sensors over the planar sensors at significantly lower applied bias. It has been demonstrated that more charge can be collected from 3D sensors than is expected to be deposited by MIPs. Charge multiplication has been shown to occur and to contribute to non-uniformities in charge collection across the unit pixel in heavily irradiated devices. TCAD simulation studies are on-going to fully investigate this phenomenon.

Acknowledgements

The authors acknowledge the funding and support of the CERN RD50 collaboration. The double-sided 3D detector development work at the University of Glasgow was supported by grants from EPSRC and STFC and by Val O'Shea and the STFC ST/G004471/1 and EPSRC EP/G005141/1 grants. The work at CNM has been partially supported by the Spanish Ministry of Education and Science through the GICSERV program "Access to ICTS integrated nano- and microelectronics cleanroom.

References

[1] C. Parkes, The LHCb upgrade, NIMA, 569 (2006) 115-118.

[2] M.G. Albrow, et al., The FP420 R&D project: Higgs and New Physics with forward protons at the LHC, JINST, 4 (2009).

[3] P. Sicho, A.P. Collaboration, SLHC upgrade plans for the ATLAS pixel detector, NIMA, 607 (2009) 31-34.

[4] G. Pellegrini, et al., First double-sided 3-D detectors fabricated at CNM-IMB, NIMA, 592 (2008) 38-43.

[5] S.I. Parker, et al., 3D -- A proposed new architecture for solid-state radiation detectors, NIMA, 395 (1997) 328-343.

[6] D. Pennicard, et al., Simulation results from double-sided 3-D detectors, ITNS, 54 (2007) 1435-1443.

[7] X. Llopart, et al., Timepix, a 65k programmable pixel readout chip for arrival time, energy and/or photon counting measurements, NIMA, 581 (2007) 485-494.

[8] X. Llopart, et al., Medipix2: a 64-k pixel readout chip with 55 μm square elements working in single photon counting mode, ITNS, 49 (2002) 2279-2283.

[9] T. Holy, et al., Data acquisition and processing software package for Medipix2, NIMA, 563 (2006) 254-258.

[10] J.J. Z. Vykydal, S. Pospisil, USB interface for Medipix2 pixel device enabling energy and position-sensitive detection of heavy charged particles, NIMA, 563 (2006) 112.

[11] Kazuyoshi Akiba, et al., Charged Particle Tracking with the Timepix ASIC, Submitted to Nucl. Instrum. Methods Phys. Res [arXiv:1103.2739v2], (2010).

[12] A. Mac Raighne, et al., Precision scans of the Pixel cell response of double sided 3D Pixel detectors to pion and X-ray beams, Journal of Instrumentation, 6 (2011).

[13] M. Koehler, et al., Beam Test Measurements With Planar and 3D Silicon Strip Detectors Irradiated to sLHC Fluences, ITNS, 58 (2011) 1308-1314.

[14] Y. Unno, et al., Development of n-on-p silicon sensors for very high radiation environments, NIMA, 636 (2011) S24-S30.

[15] http://www.iaea.or.at/worldatom/rrdb/, Technical details of the TRIGA Mark II reactor of the Jozef Stefan Institute in Ljubljana, in.

[16] A. Affolder, et al., Studies of charge collection efficiencies of planar silicon detectors after doses up to 10(15) n(eq) cm(-2) and the effect of varying diode configurations and substrate types, NIMA, 604 (2009) 250-253.

[17] M. Agari, et al., Beetle - a radiation hard readout chip for the LHCb experiment, NIMA, 518 (2004) 468-469.

[18] R. Marco-Hernandez, A. Collaboration, A Portable Readout System for Microstrip Silicon Sensors (ALIBAVA), ITNS, 56 (2009) 1642-1649.

[19] R.L. Bates, et al., Charge collection studies and electrical measurements of heavily irradiated 3D Double-Sided sensors and comparison to planar strip detectors, Submitted to IEEE Transactions on Nuclear Science.

[20] A. Zoboli, et al., Laser and beta source setup characterization of 3D-DDTC detectors fabricated at FBK-irst, NIMA, 604 (2009) 238-241.

[21] Michael Köhler, et al., Comparative measurements of highly irradiated n-in-p and p-in-n 3D silicon strip detectors, NIMA, (2011).

[22] E.N. Gimenez, et al., 3D Medipix2 detector characterization with a micro-focused X-ray beam, NIMA, 633 (2011) S114-S116.